MITSUBISHI ELECTRIC RESEARCH LABORATORIES
https://www.merl.com

Transient Simulation of Refrigerant and Oil Flow Distribution in Air Source Heat Pump Systems

Qiao, Hongtao; Miyawaki, Kosuke; Nishio, Jun; Laughman, Christopher R.

TR2025-107 July 16, 2025

Abstract

This paper presents a detailed transient simulation model to analyze the dynamic behavior of refrigerant-oil mixtures in vapor compression systems, with a particular focus on air-source heat pump operation during heating-mode cycling. A modular simulation framework is developed, incorporating refined sub-models for the compressor, heat exchangers, accumulator, and connecting tubing. Empirical correlations are applied to predict heat transfer coefficients, pressure drops, and oil retention characteristics across varying operating conditions. The simulation results reveal pronounced transient imbalances in refrigerant and oil distribution throughout the system, strongly influenced by ambient temperature variations and system cycling dynamics. These findings highlight the critical role of dynamic refrigerant-oil interaction modeling in achieving accurate system performance prediction and provide valuable insights for optimizing heat pump design and control strategies.

International Conference on Compressor and Refrigeration 2025

Mitsubishi Electric Research Laboratories, Inc.
201 Broadway, Cambridge, Massachusetts 02139

Transient Simulation of Refrigerant and Oil Flow Distribution in Air Source Heat Pump Systems

Hongtao QIAO[1,*], Kosuke MIYAWAKI[2],
Jun NISHIO[2], Christopher R. LAUGHMAN[1]
[1]Mitsubishi Electric Research Laboratories, Cambridge, MA 02139, USA
{qiao, laughman}@merl.com
[2]Mitsubishi Electric Corporation, Hyogo 661-8661, Japan
miyawaki.kosuke@da.mitsubishielectric.co.jp, nishio.jun@dp.mitsubishielectric.co.jp

Keywords: Dynamic modeling; Simulation; Lubricating oil; Heat pump; HVAC system; Modelica

Abstract This paper presents a detailed transient simulation model to analyze the dynamic behavior of refrigerant-oil mixtures in vapor compression systems, with a particular focus on air-source heat pump operation during heating-mode cycling. A modular simulation framework is developed, incorporating refined sub-models for the compressor, heat exchangers, accumulator, and connecting tubing. Empirical correlations are applied to predict heat transfer coefficients, pressure drops, and oil retention characteristics across varying operating conditions. The simulation results reveal pronounced transient imbalances in refrigerant and oil distribution throughout the system, strongly influenced by ambient temperature variations and system cycling dynamics. These findings highlight the critical role of dynamic refrigerant-oil interaction modeling in achieving accurate system performance prediction and provide valuable insights for optimizing heat pump design and control strategies.

Introduction

Vapor compression cycle-based air-source heat pump systems are widely used in residential, commercial, and industrial applications due to their high energy efficiency, environmental benefits, and operational flexibility. These systems extract heat from ambient air for heating, cooling, or water heating, playing a crucial role in sustainable building practices. Their effectiveness across diverse climatic conditions, combined with advancements in refrigerants and system designs, has driven widespread adoption.

Among the various components of a vapor compression system, the compressor serves as its heart, providing the necessary pressure rise to circulate refrigerant throughout the cycle. To ensure the proper function and longevity of the compressor, lubricating oil plays a crucial role in reducing friction and wear, maintaining pressure differentials, and dissipating heat generated during compression. However, a fraction of the oil inevitably exits the compressor and circulates with the refrigerant, influencing system performance, efficiency, and stability. Therefore, a thorough understanding of refrigerant-oil interactions is essential for optimizing heat pump operation, minimizing energy losses, and enhancing overall system reliability.

Numerous studies have explored the interactions between refrigerants and oils in vapor compression systems, focusing on oil retention, migration, and their impact on system performance. Wang et al. [1] conducted a comprehensive review and meta-analysis of oil effects in microchannel heat exchangers, synthesizing findings on how oil presence alters flow dynamics and heat transfer characteristics, while emphasizing the need for optimized oil selection. In recent years, there has been a growing interest in understanding transient refrigerant-oil behavior under dynamic operating conditions. Li and Hrnjak [2] investigated transient oil retention in a residential heat pump water heater, highlighting the importance of capturing real-time oil migration to enhance system efficiency and reliability. Similarly, Chen et al. [3] demonstrated that different lubricating oils significantly affect refrigerant charge distribution and overall system performance in R290 split air conditioners. Additionally, Lei et al. [4] examined refrigerant migration and the impact of oil sump viscosity changes in high-pressure rotary compressors, revealing that refrigerant migration during shutdown can alter oil properties, thereby influencing startup reliability.

Several studies have specifically examined oil behavior within compressors—a critical factor in ensuring reliable lubrication. For instance, Xu and Hrnjak [5] explored the formation, distribution, and movement of oil droplets in the compressor plenum, shedding light on oil dispersion mechanisms and their direct impact on lubrication performance. In parallel, research on oil charge distribution in air-conditioning heat exchangers has led to optimized oil return strategies. Jin and Hrnjak [6] developed an experimentally validated model for refrigerant and lubricant charge optimization, offering improved methods for managing oil retention and enhancing system efficiency. Similarly, Hwang et al. [7] and Wu et al. [8] investigated oil retention in transcritical CO_2 and R290 air-conditioning systems, respectively, demonstrating that both oil miscibility and system design play significant roles in determining oil return efficiency and heat exchanger performance.

Experimental visualization techniques have further enriched our understanding of oil flow within these systems. Zeng et al. [9] examined the retention and flow characteristics of R32/PVE oil in suction lines, highlighting how factors such as pipe orientation, refrigerant velocity, and gravity contribute to oil accumulation. Complementing these findings, Wang et al. [10] conducted a visualization study of oil migration in an R290 system during startup and defrost cycles, revealing that dynamic variations in oil flow can significantly influence compressor lubrication and overall system stability.

Collectively, these studies have advanced the development of more accurate refrigerant-oil interaction models and more effective oil management strategies. By addressing both steady-state and transient behaviors, researchers are continually refining system designs to enhance oil return, reduce energy losses, and ultimately improve the reliability and efficiency of vapor compression systems.

Although these advancements have led to better system designs and more efficient oil return strategies, the modeling of refrigerant-oil behavior under dynamic conditions remains scarce. Most existing models focus on steady-state conditions, overlooking the complexities introduced by transient events such as startup, shutdown, load fluctuations, and defrosting cycles. Moreover, the impact of transient events on oil return and potential oil starvation in the compressor remains insufficiently explored, highlighting the need for more detailed and robust transient simulation approaches. Capturing these dynamic interactions is crucial for accurately predicting oil migration patterns and ensuring reliable lubrication and system performance.

However, several challenges hinder the development of comprehensive transient refrigerant-oil models. First, the highly complex, multiphase nature of refrigerant-oil mixtures makes it difficult to characterize interactions between dispersed oil droplets, liquid films, and refrigerant flow patterns, especially under rapidly changing conditions. Second, transient simulations require high spatial and temporal resolutions to accurately capture phase separation, oil transport, and flow instabilities, which increases computational demands and makes real-time implementation challenging. Third, the lack of extensive experimental data for validation poses a significant limitation. Measuring oil concentration, film thickness, and migration behavior in real-world systems is difficult due to the opacity of refrigerant-oil mixtures and the need for specialized, non-intrusive diagnostic techniques. Lastly, existing models often rely on simplified assumptions regarding oil miscibility, viscosity variations, and flow regime transitions, which may not fully capture the complexities of refrigerant-oil interactions across different system configurations and refrigerant types.

Addressing these challenges requires the integration of high-fidelity simulations, advanced experimental techniques, and potentially machine learning-based predictive models. However, fully resolving these issues remains difficult due to the limited understanding of refrigerant-oil mixture behavior. Building on our previous work [11], this study refines our transient simulation framework to analyze the distribution of refrigerant-oil mixtures in heat pump systems. The proposed models incorporate thermodynamic, fluid flow, and heat transfer principles to simulate refrigerant distribution, oil accumulation, phase transitions, and their impacts on overall system performance. The remainder of this paper is structured as follows: Section 2 presents the modeling details of the system components; Section 3 discusses the simulation results; and Section 4 concludes the study.

Model Development

Refrigerant Flow Model The dynamic behavior of refrigerant-oil mixture flow is governed by conservation laws for one-dimensional flow, assuming fluid properties vary only along the flow direction and remain uniform or averaged at each cross-section. To simplify the model, the following assumptions are made: (1) refrigerant and oil are fully miscible, (2) mass-weighted reciprocal rule for density calculation, (3) oil exists only in the liquid phase with negligible vapor-phase presence, (4) axial heat conduction is ignored, (5) viscous dissipation is neglected, (6) liquid and vapor maintain thermodynamic equilibrium in two-phase regions, (7) refrigerant potential and kinetic energy are negligible, and (8) dynamic pressure waves have minimal impact on momentum conservation.

The balances of refrigerant mass, energy, oil mass and momentum are given as follows.

$$\frac{\partial(\rho A)}{\partial t}+\frac{\partial \dot{m}}{\partial z}=0 \tag{1}$$

$$\frac{\partial\left[(\rho h-p)A\right]}{\partial t}+\frac{\partial\left(\dot{m}\hat{h}\right)}{\partial z}=Pq'' \tag{2}$$

$$\frac{\partial(\rho A w)}{\partial t}+\frac{\partial(\dot{m}c)}{\partial z}=0 \tag{3}$$

$$A\frac{\partial p}{\partial z}+\tau P=0 \tag{4}$$

where w is the oil mass fraction, ρ is the mean density, c is the oil circulation rate (OCR) defined as the ratio of oil mass flow rate to the total mass flow rate, h is density-weighted specific enthalpy, and $\hat{h}$ is flow-weighed specific enthalpy.

Given that this study is to predict refrigerant and oil distribution in heat pump systems, it is important to conserve the mass of refrigerant and oil in simulations. adopting a similar approach presented in [12], redundant dynamic states are chosen to ensure density is included as a dynamic state to ensure mass conservation. Therefore, density, pressure, specific enthalpy and oil concentration are treated as dynamic states. Applying the finite volume method (FVM) to solve the governing equations requires spatial discretization of the refrigerant-oil mixture flow domain into n control volumes. A staggered grid scheme is employed to decouple the continuity and energy equations from the momentum equation. Two types of cells are defined: volume cells (enclosed by black solid lines) and flow cells (enclosed by red dashed lines), as illustrated in Fig. 1. Mass and energy balances are computed within volume cells, while the momentum balance is evaluated between volume cells, i.e., within flow cells. Integrating Eqs. (1) - (4) over the i^{th} volume cell yields

$$A\Delta z\frac{d\rho_i}{dt}=\dot{m}_{i-1/2}-\dot{m}_{i+1/2} \tag{5}$$

$$\frac{dh_i}{dt} = \left.\frac{\partial h_i}{\partial p_i}\right|_{\rho,w} \frac{dp_i}{dt} + \left.\frac{\partial h_i}{\partial \rho_i}\right|_{p,w} \frac{d\rho_i}{dt} + \left.\frac{\partial h_i}{\partial w_i}\right|_{p,\rho} \frac{dw_i}{dt} \tag{6}$$

$$A\Delta z\left(\rho_i \frac{dh_i}{dt} - \frac{dp_i}{dt}\right) = \dot{m}_{i-1/2}\left(\hat{h}_{i-1/2} - h_i\right) - \dot{m}_{i+1/2}\left(\hat{h}_{i+1/2} - h_i\right) + Pq_i''\Delta z \tag{7}$$

$$A\Delta z \rho_i \frac{dw_i}{dt} = \dot{m}_{i-1/2}\left(c_{i-1/2} - w_i\right) - \dot{m}_{i+1/2}\left(c_{i+1/2} - w_i\right) \tag{8}$$

$$p_i - p_{i+1} = \Delta p_{f,i} \tag{9}$$

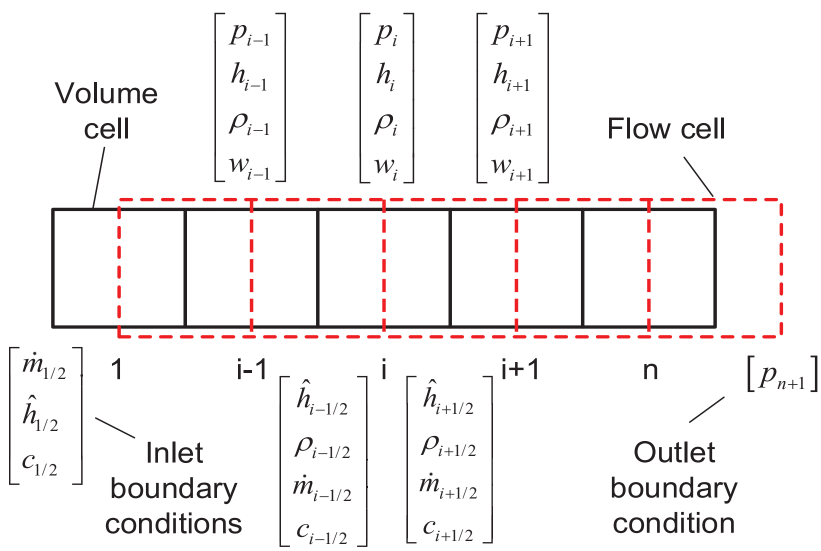

Fig. 1 FVM of refrigerant-lubricant mixture flow

It is necessary to introduce additional equations relating the quantities in volume and flow cells.

$$\varphi_{i+1/2} = \varphi_i \delta + (1-\delta)\varphi_{i+1} \tag{10}$$

For convection-dominated flows, the upwind difference scheme is recommended to approximate thermodynamic quantities onto the staggered cells, because the central difference scheme may lead to non-physical solutions [13].

$$\delta = \begin{cases} 1 \text{ when } \dot{m}_{i+1/2} \geq 0 \\ 0 \text{ when } \dot{m}_{i+1/2} < 0 \end{cases} \tag{11}$$

Therefore, one can easily obtain the flow-weighted enthalpy at the interface of the volume cells (i.e., the center of the flow cells)

$$\hat{h}_{i+1/2} = \begin{cases} \hat{h}_i \quad \text{when } \dot{m}_{i+1/2} \geq 0 \\ \hat{h}_{i+1} \text{ when } \dot{m}_{i+1/2} < 0 \end{cases} \tag{12}$$

Similarly, oil circulation rate can be related to oil mass fraction of each flow cell.

$$c_{i+1/2} = \begin{cases} \left(1-\hat{x}_{i+1/2}\right) w_i \quad \text{when } \dot{m}_{i+1/2} \geq 0 \\ \left(1-\hat{x}_{i+1/2}\right) w_{i+1} \text{ when } \dot{m}_{i+1/2} < 0 \end{cases} \tag{13}$$

where $\hat{x}$ is flow quality that is evaluated with $\hat{h}$ which can be related to density-weighted enthalpy using the Zivi slip-ratio based void fraction model [14] due to simplicity

$$\hat{h} = h + \frac{\left(\rho_f / \rho_g\right)^{1/3} - 1}{1 + x\left[\left(\rho_f / \rho_g\right)^{1/3} - 1\right]} x\left(1-x\right)\left(h_g - h_f\right). \tag{14}$$

Note that x and $\hat{x}$ are both zero for the subcooled liquid and unity for the superheated vapor, implying that these two enthalpies should be equal to each other for single-phase flows. All of the variables in Equation (14) are thermodynamic properties, and can be readily calculated except for the thermodynamic quality x.

Eqs. (6) - (9) can be numerically solved if the thermophysical properties of the refrigerant-oil mixture—particularly the phase equilibrium properties—are known. In general, the pressure–temperature–concentration relationship for a refrigerant-oil mixture can be determined using either an equation of state (EOS) with mixing rules or activity coefficient models based on Gibbs energy formulations. However, both approaches are inherently iterative and not well suited for the simulation of vapor compression cycles, where computation time is heavily influenced by thermophysical property evaluations.

To address this limitation, our study adopts iteration-free empirical correlations proposed in [15] to compute the thermodynamic properties of the refrigerant-oil mixture, including bubble point temperatures, local oil concentrations, liquid-phase specific heats, and enthalpy changes during evaporation. As a result, the added complexity is modest, and the impact on overall simulation speed is minimal.

Figure 2 illustrates the boiling process of the refrigerant-oil mixture. Depending on the stage of this process, the partial derivatives of enthalpy in Eq. (6) can be reformulated in terms of the partial derivatives of density.

$$\left.\frac{\partial h}{\partial p}\right|_{\rho,w} = -\left.\frac{\partial \rho}{\partial p}\right|_{h,w} / \left.\frac{\partial \rho}{\partial h}\right|_{p,w} \tag{15}$$

$$\left.\frac{\partial h}{\partial \rho}\right|_{p,w} = 1 / \left.\frac{\partial \rho}{\partial h}\right|_{p,w} \tag{16}$$

$$\left.\frac{\partial h}{\partial w}\right|_{p,\rho} = -\left.\frac{\partial \rho}{\partial w}\right|_{p,h} / \left.\frac{\partial \rho}{\partial h}\right|_{p,w} \tag{17}$$

It is important to note that all the aforementioned equations are also applicable to the condensation process. However, the presence of oil does not affect the calculation of the dew point temperature, since only the refrigerant is present in the vapor phase during condensation.

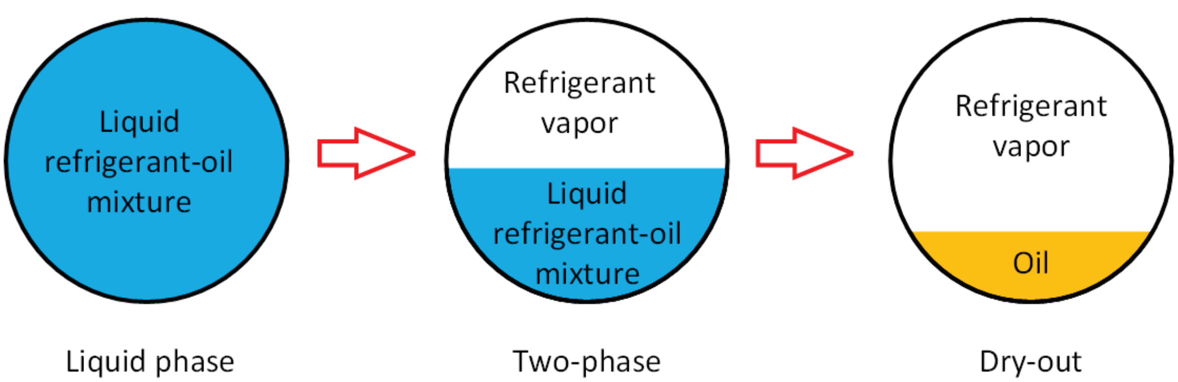

Fig. 2 Refrigerant-oil mixture boiling process

Compressor Model A variable-speed high-side scroll compressor was utilized in this study. Since performance maps for these compressors exhibit reduced accuracy when extrapolated beyond their tabulated ranges of saturated discharge and suction temperatures, we converted the performance map into a set of curve-fitted equations. This approach enhances numerical stability and prevents poor simulation behavior.

The volumetric efficiency of this compressor model is a function of the suction pressure, discharge pressure and compressor frequency

$$\eta_v = \kappa_0 + \kappa_1\varphi + \kappa_2\varphi^2 + \kappa_3\left(p_{dis} - p_{suc}\right)\left(1 + \kappa_4 p_{suc}\right) \tag{18}$$

where $\varphi = p_{dis}/p_{suc}$, $\kappa_i = a_{i,1} + a_{i,2}\varpi + a_{i,3}\varpi^2$, and $\varpi = f/f_{nom}$.

The mass flow rate is determined by

$$\dot{m}_{comp} = \eta_v f \rho_{suc} V_{disp} \tag{19}$$

The power consumed by the compressor is determined by

$$W = \zeta_1 p_{suc}\dot{V}_{suc}\left(\varphi^{\zeta_2} - \zeta_3\right) + \zeta_4 \tag{20}$$

where $\zeta_i = b_{i,1} + b_{i,2}\varpi + b_{i,3}\varpi^2$.

The enthalpy of the refrigerant leaving the compression chamber is

$$h_{comp} = \eta_{mot}\eta_{mech} W / \dot{m}_{comp} + h_{suc}\,. \tag{21}$$

In a high-side scroll compressor, after leaving the compression chamber, the high-pressure refrigerant flows radially outward through discharge ports into the compressor shell, which serves as a high-pressure reservoir. As the refrigerant circulates within the shell, it also acts as a cooling medium for the electric motor by flowing over the stator and rotor windings, dissipating heat before exiting through the discharge line. This indirect cooling mechanism helps maintain motor efficiency and prevents overheating. Inside the shell, centrifugal forces help separate some of the oil from the refrigerant, allowing it to collect at the bottom which forms an oil reservoir. A portion of this oil is recirculated back into the compression chamber through a passive pressure-driven supply mechanism, which utilizes differential pressure between the shell and the suction chamber to regulate oil flow back into the compression process, ensuring proper lubrication of the scroll elements and bearings.

The complex dynamics of refrigerant and oil flow inside the compressor shell involve multiphase interactions, heat transfer, and phase separation, as illustrated in Fig. 3. Within the shell, the refrigerant undergoes phase transitions and interacts with entrained oil droplets, influencing both thermal and fluid dynamics. To simplify the analysis, we assume a uniform shell temperature and a uniform temperature distribution across all internal metallic components. The energy balances governing these components are given by the following equations.

$$M_{sh}c_{p,sh}\frac{dT_{sh}}{dt} = \alpha_{i,sh}A_{sh}\left(T_r - T_{sh}\right) + \alpha_{o,sh}A_{sh}\left(T_{amb} - T_{sh}\right) \tag{22}$$

$$M_m c_{p,m}\frac{dT_m}{dt} = \alpha_m A_m\left(T_r - T_m\right) + \left(1 - \eta_{mot}\eta_{mech}\right)W \tag{23}$$

To ensure accurate estimation of thermal resistances, the heat transfer areas of individual metallic elements should be measured as accurately as possible, and the corresponding heat transfer coefficients are determined using empirical correlations based on the refrigerant state within the compressor shell. Specifically, during operation, the Dittus-Boelter correlation [16] is applied for single-phase convective heat transfer, while the Gungor-Winterton correlation [17] is used to estimate the two-phase heat transfer coefficient, accounting for liquid-vapor interactions in the shell. During off-periods, when natural convection and boiling effects dominate, the Churchill-Chu correlation [18] is employed for free convection heat transfer, and the Cooper correlation [19] is used to calculate the boiling heat transfer coefficient, considering nucleate boiling effects near heated surfaces. These correlations enable a more precise assessment of heat dissipation pathways within the compressor shell, ensuring a reliable thermal model for predicting refrigerant-oil behavior under various operating conditions.

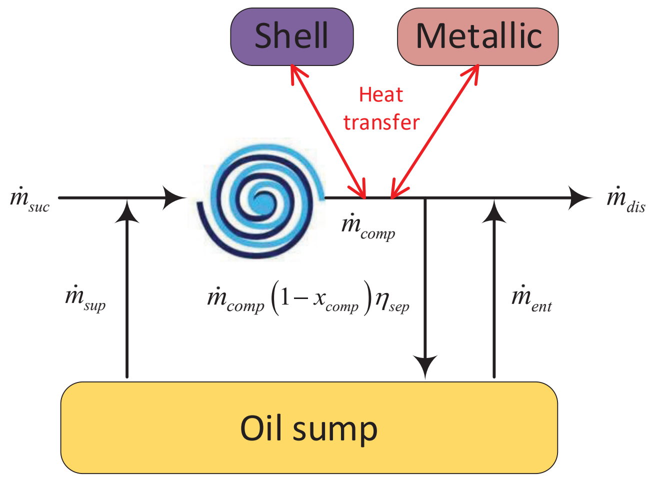

Fig. 3 Refrigerant-oil flow of a high side scroll compressor

The free volume inside the shell is modeled as a single control volume with mass and energy conservation equations formulated as

$$V\frac{d\rho}{dt} = \dot{m}_{comp} - \dot{m}_{dis} - \dot{m}_{sup} \tag{24}$$

$$V\frac{d\left(\rho h - p\right)}{dt} = \dot{m}_{comp}h_{comp} - \dot{m}_{dis}h_{dis} - \dot{m}_{sup}h_{sup} - \alpha_{i,sh}A_{sh}\left(T_r - T_{sh}\right) - \alpha_m A_m\left(T_r - T_m\right) \tag{25}$$

$$V\frac{d\left(\rho w\right)}{dt} = \dot{m}_{comp}c_{comp} - \dot{m}_{dis}c_{dis} - \dot{m}_{sup}c_{sup} \tag{26}$$

Within this control volume, the key mass flow components include:

$\dot{m}_{comp}$: Refrigerant mass flow exiting the compression chamber into the shell.

$\dot{m}_{dis}$: Refrigerant mass flow discharged through the outlet pipe.

$\dot{m}_{sup}$: Oil supplied back to the compression chamber for lubrication.

$\dot{m}_{ent}$: Oil mass flow entrained in the refrigerant flow leaving the shell.

The oil separation process within the shell is governed by complex multiphase flow interactions, including turbulent dispersion, coalescence, and gravitational settling of oil droplets. The efficiency of oil separation depends on several factors, such as refrigerant velocity, droplet size distribution, and flow path geometry. However, due to the difficulty of resolving these dynamics in a reduced-order model, the oil separation efficiency is approximated using a constant parameter that is calibrated against experimental data to ensure realistic oil return predictions.

Accumulator Model Fig. 4 illustrates the internal flow dynamics and phase separation process within the accumulator. The inlet refrigerant mixture, which contains both liquid and vapor, enters the accumulator and undergoes phase separation due to gravitational and inertial effects. The lighter vapor phase rises to the top and exits through the vapor outlet, ensuring only vapor is supplied to the compressor.

The liquid phase collects at the bottom, where a small metering orifice controls the regulated return of liquid refrigerant and oil back into the suction line.

The accumulator was modeled as a lumped control volume incorporating the following simplifications: (1) Ideal Phase Separation: Liquid and vapor phases are assumed to separate perfectly within the accumulator; (2) Thermodynamic Equilibrium: The refrigerant inside the tank is considered to be in thermodynamic equilibrium, meaning the liquid and vapor phases share the same temperature and pressure; and (3) Adiabatic Assumption: Heat exchange with the surroundings is neglected, assuming that the tank is thermally insulated.

Under these assumptions, the governing equations for mass and energy conservation follow the same form as Eqs. (24) - (26), with modifications to the source terms on the right-hand side to account for phase separation dynamics. The refrigerant mass flow exiting the accumulator is determined using a stream analysis [20], which balances the internal pressures and regulates the flow of vapor and liquid. As indicated in Fig. 4, there are five distinct refrigerant streams within the accumulator:

Stream 1: Flow from the top of the J-tube pipe to the oil bleed hole.
Stream 2: Flow through the oil bleed hole into the J-tube pipe.
Stream 3: Flow through the anti-siphon hole into the J-tube pipe.
Stream 4: Flow within the J-tube pipe from the oil bleed hole to the anti-siphon hole.
Stream 5: Flow leaving the J-tube pipe and exiting the accumulator.

The mass balances for these streams can be formulated as:

$$\dot{m}_1 + \dot{m}_2 = \dot{m}_4 \tag{27}$$

$$\dot{m}_3 + \dot{m}_4 = \dot{m}_5 \tag{28}$$

To determine the flow rate of each stream, an iterative solution of pressure drop equations (29) is required. The calculations account for various factors, including sudden expansion and contraction effects, liquid height variations, and frictional pressure losses within the J-tube. The interaction between these five streams plays a critical role in regulating oil return, ensuring proper lubrication of the compressor while preventing excessive oil carryover into the system.

$$\begin{gathered} \dot{m}_1 = f\left(p_a - p_{b,int}\right), \dot{m}_2 = f\left(p_{b,ext} - p_{b,int}\right), \\ \dot{m}_3 = f\left(p_{c,ext} - p_{c,int}\right), \dot{m}_4 = f\left(p_{b,int} - p_{c,int}\right), \dot{m}_5 = f\left(p_{c,int} - p_d\right) \end{gathered} \tag{29}$$

Expansion Valve Model The system incorporates an electronic expansion valve (EEV) to regulate refrigerant flow. The mass flow rate through the valve is modeled using a standard orifice-type relationship, which correlates mass flow rate with the pressure drop across the valve. This approach is commonly used in refrigeration and air conditioning systems to capture the flow characteristics of metering devices. The mass flow rate through the EEV is given by:

$$\dot{m} = C_v \sqrt{\rho_{in} \Delta p} \tag{30}$$

The flow coefficient C_v varies with the valve opening and is characterized by experimental measurements to ensure accurate representation of the valve's flow behavior.

Implementation The balance equations governing mass, momentum, and energy conservation were supplemented with a set of empirical closure relations to describe both single-phase and two-phase heat transfer coefficients as well as frictional pressure drops on the refrigerant and air sides. These closure relations ensure accurate predictions of heat exchanger performance and pressure losses within the system. To capture the detailed thermodynamic interactions in heat exchangers, a tube-by-tube analysis approach was employed [21]. Each tube was treated as an independent control volume, allowing for localized variations in refrigerant properties, air mass flow rate, inlet temperature, and humidity. This approach ensures that spatial variations in heat transfer and fluid flow are properly accounted for, enhancing model fidelity. The system models were implemented using the Modelica language in the Dymola 2024x simulation environment. Modelica's object-oriented, equation-based, and acausal modeling capabilities facilitated the modular development of individual component models, which were then interconnected to form a complete system representation. Refrigerant properties were computed using a B-spline interpolation method [22], providing computationally efficient and accurate thermodynamic property calculations. Simulations were executed on a laptop equipped with an Intel i7 processor and 16 GB of RAM. The DASSL solver was employed for numerical integration of the system's differential-algebraic equations (DAEs) with a solver tolerance of 10^{-6}, ensuring high numerical accuracy and stability.

Results and Discussion

To verify the efficacy of the proposed models, a detailed simulation of an air source heat pump (ASHP) cycle was conducted to capture the transient behavior of refrigerant and oil during cycling operations. The system employed R32 as the working fluid and consisted of an indoor coil, an outdoor coil, an accumulator, a scroll compressor, and an electronic expansion valve, as illustrated in Fig. 5. A high-side scroll compressor was used to drive refrigerant circulation throughout the system. The electronic expansion valve modulated refrigerant flow based on a control loop that maintained a target suction superheat.

Simulations were performed under heating-mode conditions, with the indoor air inlet temperature fixed at 21°C and the outdoor ambient temperature varied across three values: 8.3°C, 1.1°C, and -5.0°C. Five test cases were evaluated, each with a unique combination of ambient temperature and compressor frequency: Case 1: 8.3°C and 50 Hz; Case 2: 1.1°C and 50 Hz; Case 3: -5.0°C and 50 Hz; Case 4: 8.3°C and 80 Hz; Case 5: 8.3°C and 30 Hz.

For simplicity, an open-loop control scheme was employed in all cases, where the EEV opening was fixed throughout each simulation. This setup enabled a consistent analysis of transient behaviors without additional control-induced variability.

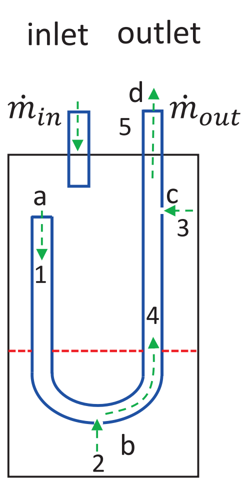

Fig. 4 Flow stream in accumulator
a – J-tube inlet, b – oil bleed hole,
c – anti-siphon hole, d - outlet

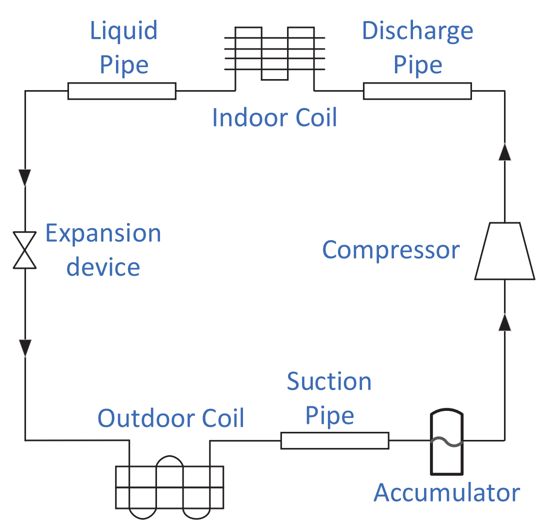

Fig. 5 Air source heat pump system

The simulations captured both cold start-up and off-cycle dynamics. The system was assumed to be off for an extended period of 45,000 seconds to allow it to reach thermodynamic equilibrium. During this phase, the refrigerant was predominantly superheated in the indoor coil, while a two-phase mixture was present in the outdoor coil. Simulation results are presented starting from 44,000 seconds to provide context leading up to the startup event. The system was activated at 45,000 seconds and operated for 5,000 seconds before being shut down at 50,000 seconds. Post-shutdown (off-cycle) behavior is illustrated over a 4,000-second window, although additional data were collected over a longer duration. The total refrigerant and lubricating oil charges were set to 1070 g and 330 g, respectively.

The pressure transients for Case 1 are shown in Fig. 6a. Prior to system activation, the discharge and suction pressures were equal, indicating equilibrium. Upon startup, the two pressures rapidly diverged, with the discharge pressure increasing and the suction pressure decreasing. Approximately 30 minutes after activation, both pressures approached their respective steady-state values. During this transient phase, the suction pressure exhibited a noticeable dip due to the compressor drawing refrigerant more rapidly than it was replenished from the high-pressure side. After the system was shut down, the discharge and suction pressures quickly converged and fully equalized within approximately 10 minutes.

As shown in Fig. 6b, there was no measurable positive suction superheat prior to system startup, indicating the presence of saturated or two-phase refrigerant at the compressor inlet. Suction superheat did not appear until approximately 10 minutes after the system was turned on, after which it gradually increased and stabilized at a steady-state value of approximately 17 K. Following system shutdown, the suction superheat briefly spiked before gradually declining to zero, again signaling a two-phase mixture at the compressor suction. Throughout the operation, the suction vapor quality remained below unity, indicating incomplete vaporization at the evaporator outlet. This apparent contradiction - high superheat values coexisting with wet vapor conditions - can be attributed to the influence of oil on the thermodynamic behavior of the refrigerant. The presence of lubricating oil elevates the local boiling point of the refrigerant due to its non-ideal mixing behavior, where the strong molecular interactions between the refrigerant and oil molecules reduce the refrigerant's partial vapor pressure, requiring a higher temperature for phase change to occur at a given pressure. The refrigerant-oil mixture behaves as a zeotropic blend with a significant temperature glide, causing the local bubble point temperature to rise as the oil concentration increases, particularly in the latter stages of the evaporator. As a result, the refrigerant can exit the evaporator at a relatively high temperature while still existing in a two-phase (wet) state.

The transients of airside heat loads and compressor power are presented in Fig. 6c. During the off-cycle, both the indoor and outdoor coils exhibited negligible heat transfer, with heat loads approaching zero. Once the system was activated, the indoor coil delivered approximately 3.5 kW of heat rejection, while the outdoor coil absorbed around 2.9 kW of heat. The compressor power consumption stabilized at approximately 0.85 kW. The discrepancy between the heat transfer rates —commonly referred to as the energy imbalance — can be attributed to thermal energy exchange within connecting pipes and compresor shell, which temporarily store or release heat during transients.

The refrigerant distribution across various system components is shown in Fig. 6d. During the off-cycle, the majority of the refrigerant—approximately 75%—resided in the outdoor coil, where it predominantly existed as a two-phase mixture. In contrast, the indoor coil stored a minimal amount of refrigerant (less than 5%), as the refrigerant in that section was in the vapor phase. The rest of the refrigerant was stored in the accumulator and connecting pipes. Upon system startup, a significant redistribution of refrigerant occurred. The compressor actively pumped refrigerant from the low-pressure side back into the indoor coil, resulting in a major shift in refrigerant inventory. During steady-state operation, approximately 55% of the refrigerant was concentrated in the indoor coil, while the outdoor coil retained only about 15%. The piping system also accounted for a substantial portion of refrigerant storage—about 25%—largely due to the presence of a 5-meter-long liquid line. The remaining refrigerant, roughly 10%, was distributed between the accumulator and the compressor. After shutdown, refrigerant quickly migrated from the high-pressure side to the low-pressure side, driven by pressure differentials, leading to a return to the pre-startup distribution pattern.

Oil retention in various system components is illustrated in Fig. 6e. During the off-cycle, the majority of the oil was retained in the compressor and accumulator, with each accounting for approximately 40% of the total oil charge. The remaining oil was distributed among the outdoor coil (~10%), indoor coil, and piping. Upon system startup, the oil content in the accumulator decreased rapidly as oil was drawn into the compressor. Over time, the oil inventory in the compressor also began to decline, indicating that a portion of the oil was being discharged and redistributed throughout the system. As steady-state conditions were approached, the oil circulation rate stabilized at approximately 2.9%, reflecting the dynamic equilibrium between oil retention and transport across components.

Refrigerant and oil distributions for Case 2 are illustrated in Fig. 6f and Fig. 6g. The only difference between Cases 1 and 2 is the lower ambient temperature in Case 2. Compared to Case 1, the amount of refrigerant stored in the indoor coil during the on-cycle is reduced in Case 2, primarily due to a lower condensing pressure that leads to decreased refrigerant density. Conversely, refrigerant accumulation in the outdoor coil increases, as reduced evaporation results in a larger proportion of two-phase flow. The oil distribution patterns remain largely consistent between the two cases, with the compressor and accumulator continuing to retain the majority of the oil. However, under the even colder ambient conditions of Case 3, the refrigerant stored in the outdoor coil during operation surpasses that in the indoor coil. Similarly, the oil content in the accumulator exceeds that in the compressor, indicating a tendency for oil to accumulate in low-pressure components under lower ambient temperatures. In contrast, the off-cycle refrigerant and oil distributions show minimal variation across different ambient conditions, as depicted in Fig. 6h and Fig. 6i. These results collectively indicate that lower ambient temperatures promote increased refrigerant and oil retention in low-side components, particularly the outdoor coil and accumulator.

Refrigerant and oil distributions for Cases 4 and 5, which represent different compressor speeds, are shown in Fig. 6j through Fig. 6m. Compared to Case 1, it is observed that increasing the compressor speed results in a higher amount of oil retained in the compressor. This trend suggests that elevated speeds enhance oil return to the compressor, likely due to stronger suction forces and increased mass flow rates, which improve oil recirculation within the system.

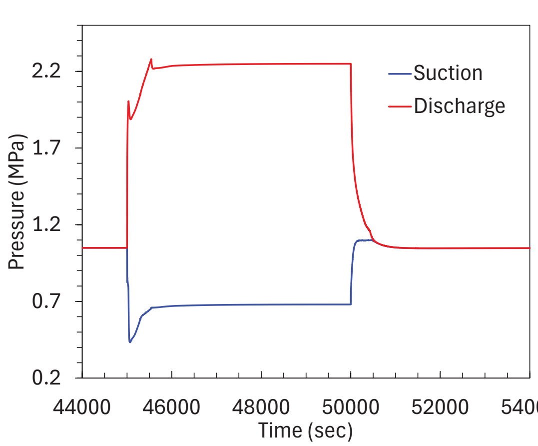

(a)

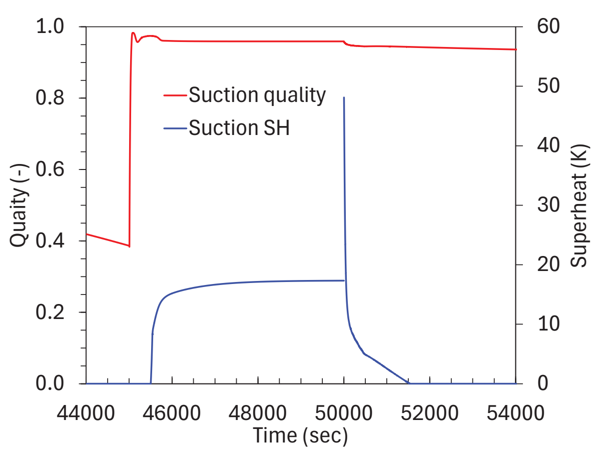

(b)

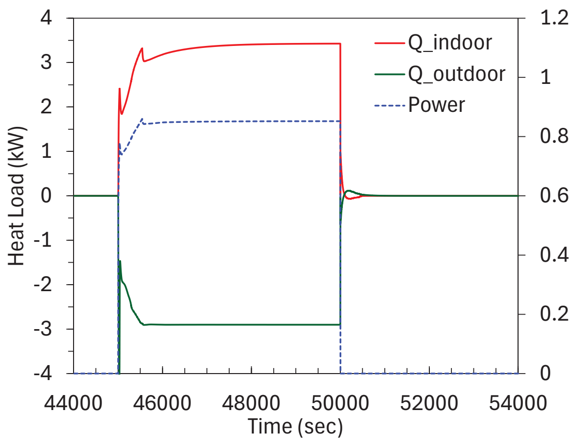

Q_indoor
Q_outdoor
Power
Heat Load (kW)
Power (kW)
Time (sec)
4
3
2
1
0
-1
-2
-3
-4
1.2
1
0.8
0.6
0.4
0.2
0
44000
46000
48000
50000
52000
54000

(c)

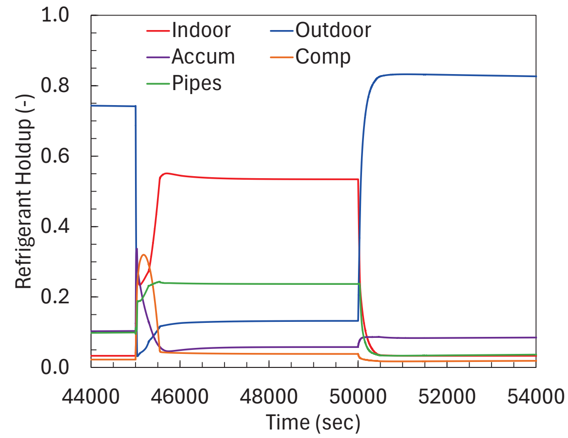

Indoor
Outdoor
Accum
Comp
Pipes
Refrigerant Holdup (-)
Time (sec)
1.0
0.8
0.6
0.4
0.2
0.0
44000
46000
48000
50000
52000
54000

(d)

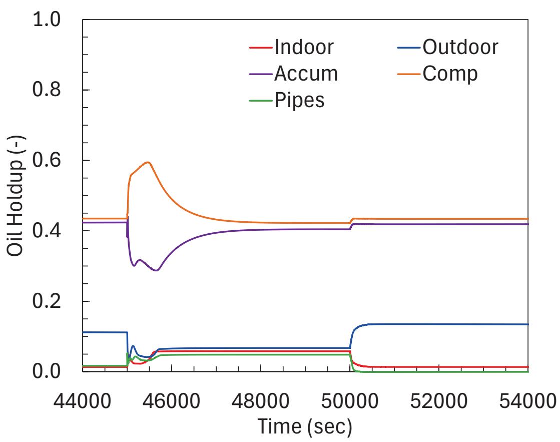

Indoor
Outdoor
Accum
Comp
Pipes
Oil Holdup (-)
Time (sec)
1.0
0.8
0.6
0.4
0.2
0.0
44000
46000
48000
50000
52000
54000

(e)

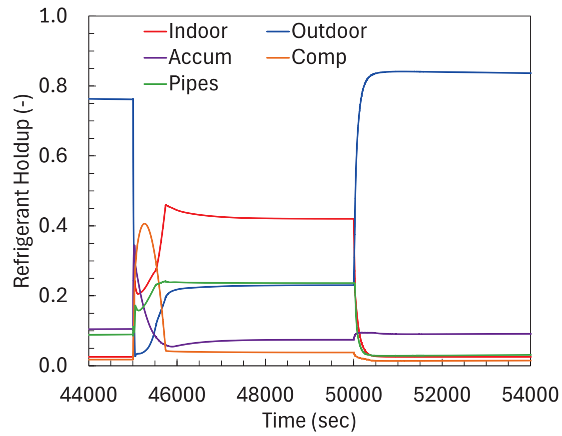

Indoor
Outdoor
Accum
Comp
Pipes
Refrigerant Holdup (-)
Time (sec)
1.0
0.8
0.6
0.4
0.2
0.0
44000
46000
48000
50000
52000
54000

(f)

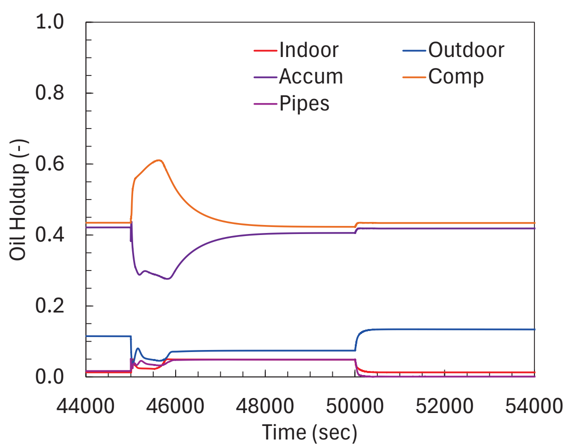

Indoor
Outdoor
Accum
Comp
Pipes
Oil Holdup (-)
Time (sec)
1.0
0.8
0.6
0.4
0.2
0.0
44000
46000
48000
50000
52000
54000

(g)

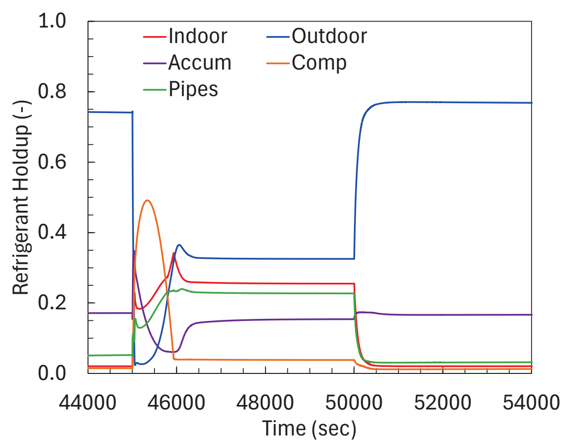

Indoor
Outdoor
Accum
Comp
Pipes
Refrigerant Holdup (-)
Time (sec)
1.0
0.8
0.6
0.4
0.2
0.0
44000
46000
48000
50000
52000
54000

(h)

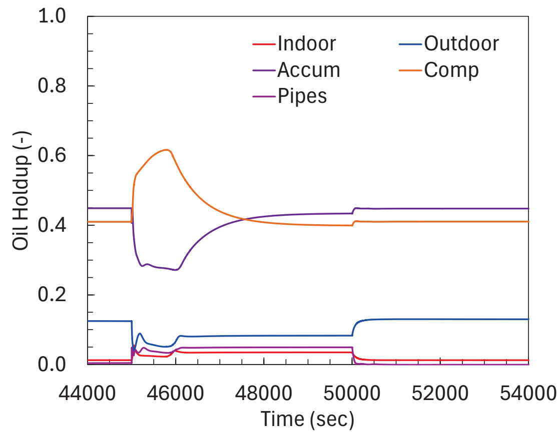

(i)

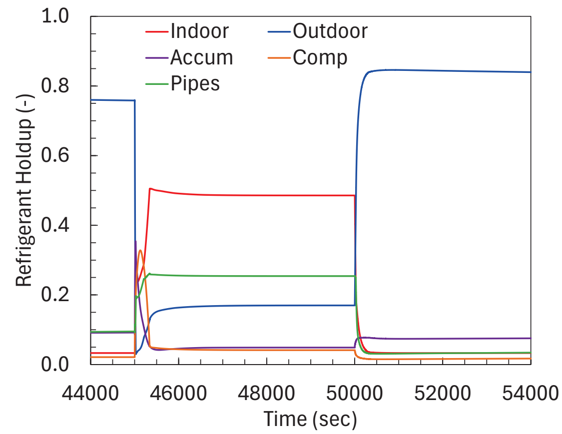

(j)

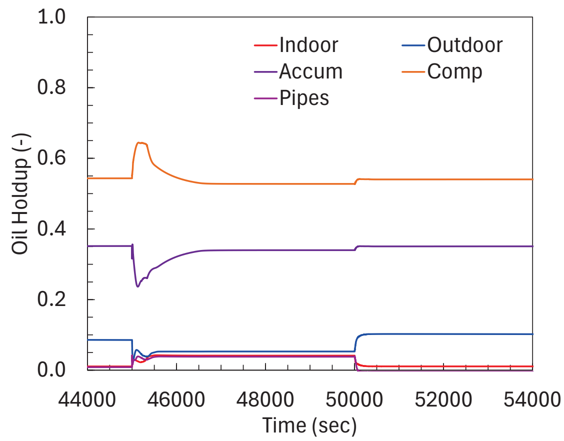

(k)

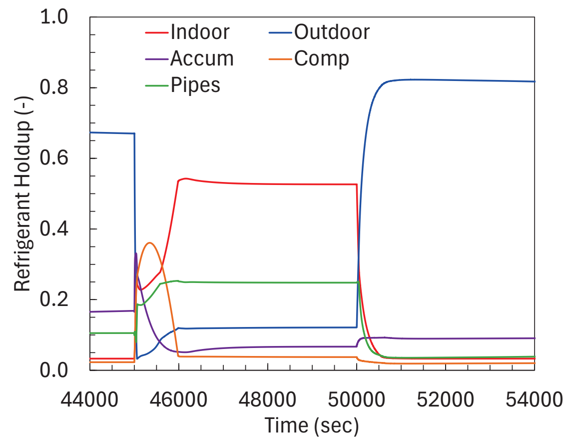

(l)

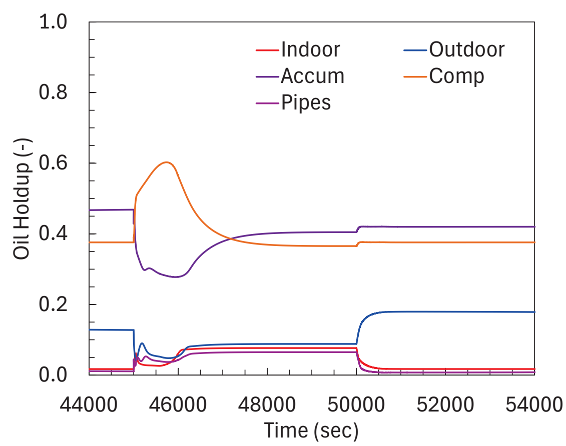

(m)

Fig. 6 Cycling transients of the ASHP: (a) pressures (case 1) , (b) suction superheat and suction quality (case 1), (c) heat loads and power (case 1), (d) refrigerant distribution (case 1), (e) oil distribution (case 1), (f) refrigerant distribution (case 2), (g) oil distribution (case 2), (h) refrigerant distribution (case 3), (i) oil distribution (case 3), (j) refrigerant distribution (case 4), (k) oil distribution (case 4), (l) refrigerant distribution (case 5), (m) oil distribution (case 5)

Conclusion

This study investigated the transient behavior of refrigerant and oil flow distribution in an air-source heat pump system under various heating-mode conditions, focusing on cold start-up and shutdown dynamics. Simulations across five test cases—with varying ambient temperatures and compressor frequencies—revealed that system start-up leads to rapid pressure divergence, delayed superheat formation, and significant redistribution of refrigerant and oil. Lower ambient temperatures increased refrigerant and oil retention in low-pressure components, especially the outdoor coil and accumulator, while higher compressor speeds enhanced oil return to the compressor. The presence of oil was found to alter refrigerant thermodynamic behavior, resulting in high superheat coexisting with wet vapor due to elevated local boiling points. These findings emphasize the critical role of ambient conditions, compressor speed, and refrigerant-oil interactions in shaping transient performance, and highlight the need to account for these factors in system design and control. Future work will focus on experimental validation and extension to other operating modes, such as frost and defrost cycles.

Nomenclature

Symbols		***Subscripts***	
A	cross sectional area	amb	ambient
c	oil circulation rate	comp	compression
c_p	specific heat	dis	discharge
f	frequency	ent	entrainment
h	specific enthalpy	ext	external
M	mass	f	liquid
$\dot{m}$	mass flow rate	g	gas
P	perimeter	i	interior
p	pressure	in	inlet
q''	heat flux	int	internal
T	temperature	m	metallic parts
t	time	mech	mechanical
V	volume	mot	motor
$\dot{V}$	volumetric flow rate	nom	nominal
W	power	o	outside
w	oil mass fraction	r	refrigerant
x	quality	sep	separation
α	heat transfer coefficient	sh	shell
η	efficiency	suc	suction
ρ	density	sup	supply
τ	wall shear stress	v	volumetric

References

[1] Q. Wang, D. Su, M. Li et al., Effects of lubricating oil on flow and heat transfer characteristics in microchannel: A systematic review and meta-analysis. Int. J. Heat Mass Transfer 235 (2024) 126199.

[2] W. Li, P. Hrnjak, Transient refrigerant and oil distribution in a residential heat pump water heater system: Experiments and model. Int. J. Refrigeration 129 (2021), 184-193.

[3] R. Chen, J. Wu, J. Duan, Performance and refrigerant mass distribution of a R290 split air conditioner with different lubricating oils. Appl. Thermal Eng. 162 (2019) 114224.
[4] B. Lei, C. Wang, J. Duan et al., Refrigerant migration and oil sump viscosity change of R290 high-pressure rotary compressor during shutdown process. Int. J. Refrigeration 136 (2022) 53-60.
[5] J. Xu, P. Hrnjak, Formation, distribution, and movement of oil droplets in the compressor plenum. Int. J. Refrigeration 93 (2018) 184-194.
[6] S. Jin, P. Hrnjak, Refrigerant and lubricant charge in air condition heat exchangers: Experimentally validated model. Int. J. Refrigeration 67 (2016) 395-407.
[7] Y. Hwang, J. Lee, R. Radermacher, Oil distribution in a transcritical CO_2 air-conditioning system. Appl. Thermal. Eng. 27 (2007) 2618-2625.
[8] J. Wu, Z. Chen, R. Chen et al., Oil retention and its mass distribution within a R290 room air conditioner using miscible or partially miscible oils. Int. J. Refrigeration 111 (2020) 20-28.
[9] W. Zeng, Z. Zhang, J. Hu et al., Visualization study on oil retention and flow characteristics of R32/PVE oil in suction lines with different flow orientations. Int. J. Refrigeration 140 (2022) 90-102.
[10] C. Wang, J. Wu, B. Lei et al., Visualization study on the flow and migration characteristics of R290/PAG oil in a room air conditioner during startup and defrosting processes. Int. J. Refrigeration 150 (2023) 149-157.
[11] H. Qiao, C.R. Laughman, Dynamic modeling of oil transport in vapor compression systems. 19th International Refrigeration and Air Conditioning Conference, Paper 2352, 2022.
[12] C.R. Laughman, H. Qiao, On the influence of state selection on mass conservation in dynamic vapour compression cycle models. Mathematical and Computer Modeling of Dynamical Systems 23 (2017) 262–283.
[13] S.V. Patankar, Numerical heat transfer and fluid flow. New York: Hemisphere Publishing Corporation, Taylor and Francis Group, 1980.
[14] S.M. Zivi, Estimation of steady-state steam void-fraction by means of the principle of minimum entropy production. J. Heat Trans-T ASME 86 (1964) 247-52.
[15] J.R. Thome, Comprehensive thermodynamic approach to modeling refrigerant-Lubricating oil mixtures. HVAC&R Res. 1 (1995) 110-125.
[16] F.W. Dittus, L.M.K., Boelter, Heat transfer in automobile radiators of the tubular type. Int. Commun. Heat. Mass Transf. 12 (1985) 3-22.
[17] K.E. Gungor, R.H.S. Winterton, Simplified general correlation for saturated flow boiling and comparisons of correlations with data. Chem. Eng. Res. Des. 65 (1987) 148-156.
[18] S.W. Churchill, H.H.S. Chu, Correlating equations for laminar and turbulent free convection from a vertical plate. Int. J. Heat. Mass Transf. 18 (1975) 1323-1329.
[19] M.G. Cooper, Saturation nucleate pool boiling: a simple correlation. In: 1st U.K. National Conference on Heat Transfer 2 (1984) 785-793.
[20] S. Wang, J. Gu, T. Dickson, Modeling and experimental investigation of accumulators for automative air conditioning systems. Int. J. Refrigeration 29 (2006) 1109-1118.
[21] H. Qiao, V. Aute, R. Radermacher, Transient modeling of a flash tank vapor injection heat pump system - part I: model development, Int. J. Refrigeration 49 (2015) 169–182.
[22] C.R. Laughman, H. Qiao, Patch-based thermodynamic property models for the subcritical Region. 18th International Refrigeration and Air Conditioning Conference at Purdue, Paper 2258, 2021.